



Global carbon
monoxide products

J. X. Warner et al.

This discussion paper is/has been under review for the journal Atmospheric Chemistry and Physics (ACP). Please refer to the corresponding final paper in ACP if available.

Global carbon monoxide products from combined AIRS, TES and MLS measurements on A-train satellites

J. X. Warner¹, R. Yang¹, Z. Wei¹, F. Carminati^{1,5,7}, A. Tangborn², Z. Sun³,
W. Lahoz^{4,5}, J.-L. Attié^{5,6,7}, L. El Amraoui⁵, and B. Duncan⁸

¹Department of Atmospheric & Oceanic Science, University of Maryland, 3433 Computer & Space Sciences Bldg, College Park, MD, USA

²Joint Center for Earth Systems Technology, University of Maryland Baltimore County, Baltimore, MD, USA

³Universities Space Research Association, 10211 Wincopin Circle, Columbia, MD 21044, USA

⁴Norwegian Institute of Air Research, Instituttveien 18, Kjeller 2027, Norway

⁵CNRM-GAME, Météo-France and CNRS, UMR3589, Toulouse, France

⁶Laboratoire d'Aérodynamique, CNRS, UMR5560, Toulouse, France

⁷Université de Toulouse, Toulouse, France

⁸Atmospheric Chemistry and Dynamics Laboratory, NASA Goddard Space Flight Center, Greenbelt, MD, USA

Title Page

Abstract

Introduction

Conclusions

References

Tables

Figures

◀

▶

◀

▶

Back

Close

Full Screen / Esc

Printer-friendly Version

Interactive Discussion



Received: 6 April 2013 – Accepted: 22 May 2013 – Published: 11 June 2013

Correspondence to: J. X. Warner (juying@atmos.umd.edu)

Published by Copernicus Publications on behalf of the European Geosciences Union.

ACPD

13, 15409–15441, 2013

**Global carbon
monoxide products**

J. X. Warner et al.

Title Page

Abstract

Introduction

Conclusions

References

Tables

Figures



Back

Close

Full Screen / Esc

Printer-friendly Version

Interactive Discussion



Abstract

This study tests a novel methodology to add value to satellite datasets. This methodology, data fusion, is similar to data assimilation, except that the background model-based field is replaced by a satellite dataset, in this case AIRS (Atmospheric Infrared Sounder) carbon monoxide (CO) measurements. The observational information comes from CO measurements with lower spatial coverage than AIRS, namely, from TES (Tropospheric Emission Spectrometer) and MLS (Microwave Limb Sounder). We show that combining these datasets with data fusion uses the higher spectral resolution of TES to extend AIRS CO observational sensitivity to the lower troposphere, a region especially important for air quality studies. We also show that combined CO measurements from AIRS and MLS provide enhanced information in the UTLS (upper troposphere/lower stratosphere) region compared to each product individually. The combined AIRS/TES and AIRS/MLS CO products are validated against DACOM (differential absorption mid-IR diode laser spectrometer) in situ CO measurements from the INTEX-B (Intercontinental Chemical Transport Experiment: MILAGRO and Pacific phases) field campaign and in situ data from HIPPO (HIAPER Pole-to-Pole Observations) flights. The data fusion results show improved sensitivities in the lower and upper troposphere (20–30% and above 20 %, respectively) as compared with AIRS-only retrievals, and improved coverage compared with TES and MLS CO data.

1 Introduction

Atmospheric carbon monoxide (CO) is simultaneously measured by three EOS (Earth Observing System) “A-train” satellite sensors: AIRS (Atmospheric Infrared Sounder) (Aumann et al., 2003) on Aqua, and TES (Tropospheric Emission Spectrometer) (Beer et al., 2006), and MLS (Microwave Limb Sounder) (Waters et al., 2006) on Aura. Based on the heritage of the A-train system with individual sensors taking measurements within short time intervals between each other (15–30 min), the combined datasets

ACPD

13, 15409–15441, 2013

Global carbon monoxide products

J. X. Warner et al.

Title Page

Abstract

Introduction

Conclusions

References

Tables

Figures

◀

▶

◀

▶

Back

Close

Full Screen / Esc

Printer-friendly Version

Interactive Discussion



Global carbon monoxide products

J. X. Warner et al.

Title Page

Abstract

Introduction

Conclusions

References

Tables

Figures

◀

▶

◀

▶

Back

Close

Full Screen / Esc

Printer-friendly Version

Interactive Discussion



from these sensors are expected to provide three-dimensional composition information that incorporates the uniqueness of AIRS large spatial coverage, TES high spectral resolution, and MLS measurements in the upper troposphere and stratosphere. AIRS trace gas retrieval products provide high-density twice-daily global coverage with spatial resolution at $45 \times 45 \text{ km}^2$ at 01:30 a.m. and 01:30 p.m. local time overpasses. However, as in the case of other nadir sounders, it lacks sensitivity for vertical structures in the UTLS (Upper Troposphere and Lower Stratosphere) regions for most chemical species. The Aura limb sounders (TES and MLS), on the other hand, possess the advantage of high vertical resolution in the UTLS region but lack horizontal coverage. We seek to combine these two types of CO datasets to provide more detail in both vertical structures and global coverage. This fused dataset will benefit studies of stratosphere troposphere exchange and the chemical and dynamical structures of the UTLS and TTL (Tropical Tropopause Layer) regions as CO is a transport tracer and has markedly different concentrations in the troposphere and the stratosphere.

Interactions between dynamics and chemistry in the region of the extratropical tropopause play a significant role in chemistry-climate coupling. Concentrations of several radiatively significant trace constituents, such as ozone and water vapor, change rapidly across the tropopause. Their gradients and variability in this region are controlled by their respective sources and sinks and the mixing and exchange between the stratosphere and the troposphere. The CO-Ozone correlation has been used extensively in the UTLS region as a diagnostic tool for extratropical tropopause processes, and stratosphere troposphere exchange and mixing (e.g., Zahn and Brenninkmeijer, 2003; Hoor et al., 2002, 2004; Pan et al., 2004, 2007a, b). UTLS dynamics and transport studies will greatly benefit from trace gas datasets that show detailed structures of CO plumes, have high-density daily global coverage, and provide information for an extended time period ($\sim 10 \text{ yr}$).

A key societal issue is air quality (AQ), which affects human health and has a significant impact on economical and policy issues (Lahoz et al., 2012). Air quality concerns span from the local to the global scales since pollution can be transported across con-

Global carbon monoxide products

J. X. Warner et al.

Title Page

Abstract

Introduction

Conclusions

References

Tables

Figures

◀

▶

◀

▶

Back

Close

Full Screen / Esc

Printer-friendly Version

Interactive Discussion



tinents and affect AQ at remote locations (Lin et al., 2011). Satellite measurements are among the most effective ways to monitor air pollution and the related transport due to the relatively high spatial and temporal coverage. CO is a good tracer of pollution emission and transport in the troposphere owing to its lifetime of 1–3 months (Crutzen and Zimmermann, 1991; Sze, 1977). In this study, we focus on CO measurements. We show that fusing of CO data from multiple sensors in space can benefit both air quality and climate studies.

In the following sections, we present the data fusion approach that we use to combine AIRS, TES, and MLS CO datasets, with TES and MLS CO as observations and AIRS CO retrievals as the instantaneous background field. We also show that the combined dataset provides a 3-D CO field with daily global coverage that incorporates the sensitivity from AIRS primarily in the mid-troposphere, TES in the lower troposphere, and MLS in the UTLS. Section 2 introduces the datasets that we use in this study, and Sect. 3 describes the data fusion methodology. Section 4 presents results and their validation, while Sect. 5 provides discussion and a summary of this study.

2 Observational data sets

The AIRS instrument on Aqua was launched in 2002 with the primary goal of determining the vertical profiles of temperature and water vapor in the Earth's atmosphere (Aumann et al., 2003). CO retrievals are obtained from the 2160–2200 cm^{-1} portion of the spectrum on the edge of the 1–0 vibration-rotation band of CO (McMillan et al., 2005). The AIRS main CO sensitivity is broad and centered in the mid troposphere between approximately 300–600 hPa (Warner et al., 2007). AIRS science team retrieval codes are used to determine the physical parameters measured by AIRS such as temperature, water vapor, and ozone (Susskind et al., 2003).

The TES instrument is an imaging infrared Fourier Transform Spectrometer with both nadir and limb-viewing capability covering the spectral range 650–3050 cm^{-1} at either 0.08 cm^{-1} or 0.02 cm^{-1} spectral resolution. TES provides higher spatial and spectral

Global carbon monoxide products

J. X. Warner et al.

Title Page

Abstract

Introduction

Conclusions

References

Tables

Figures

◀

▶

◀

▶

Back

Close

Full Screen / Esc

Printer-friendly Version

Interactive Discussion



resolutions compared to AIRS; however, the global coverage of TES is significantly lower (Luo et al., 2002, 2007). This is partly due to the fact that, in addition to the sensors' respective swath widths, AIRS uses a cloud-clearing scheme that recovers, on the average, more than half of the cloudy pixels, which increases the global coverage of the retrievals significantly (Susskind et al., 2003).

MLS on Aura satellite was launched on 15 July 2004 and placed into a near-polar Earth orbit at ~ 705 km with an inclination of 98° and an ascending node at 13:45 h local time. It makes about 14 orbits per day. The MLS instrument onboard Aura uses the microwave limb sounding technique to measure chemical constituents and dynamical tracers between the upper troposphere and the lower mesosphere. It provides dense spatial coverage with 3500 profiles daily between 82° N and 82° S. The standard retrievals for CO are given between 215 and 0.46 hPa with a vertical resolution of ~ 3 km in the upper troposphere and the stratosphere. The along-track resolution of CO is ~ 200 km between 215 and 10 hPa. The estimated single-profile precision in the extra tropical UTLS is of the order of 0.04 ppmv (parts per million volume) from 215 to 100 hPa and between 0.05 and 0.2 ppmv from 46 to 10 hPa (Livesey et al., 2007; Read et al., 2007; Jiang et al., 2007).

3 Methodology

The data fusion methodology in this study takes a similar approach to that used in data assimilation (Kalnay, 2003) except we use AIRS measurements as the background field and other measurements with lower spatial coverage (in this case, TES and MLS) as the observations. We assume that the AIRS data represent a snapshot of a three dimensional geophysical field analogous to a model output. We do not attempt to evaluate any time variability in the CO field, but to simply combine a number of measurements taken within a short time period (15–30 min). A major difference between this technique and traditional data assimilation is that we do not use a model, which avoids uncertainties arising from model dynamics and transport issues. We follow a formu-

lation identical to the Kalman filter method, commonly used in data assimilation (e.g. Lahoz et al., 2010), except we exclude the transport by model dynamics.

The diagram in Fig. 1 illustrates the data fusion system, where we start with AIRS operational V5 L2 retrievals, shown on the upper left corner, as the background. Other products, such as TES or MLS, are added to the Kalman filter process as observations where the relative weighting is influenced by the error covariance from AIRS and TES or MLS retrievals. The output from the analysis provides a three-dimensional field that incorporates measurements from AIRS, TES, and MLS. The population of the profiles on the horizontal plane is determined primarily by the observed variances from the background field provided by AIRS. We show that in the vertical region (lower troposphere and the UTLS) where AIRS has low measurement sensitivity, the AIRS retrievals still provide the correct spatial variability (or spatial patterns), even when they cannot reproduce the correct CO magnitude. This system does not require a model to constrain the physics of the geophysical fields, but rather uses AIRS continuous measurements to constrain the spatial and temporal variability of the TES and MLS measurements.

The Kalman filter algorithm in general form is as follows

$$\mathbf{X}^a = \mathbf{X}^b + \mathbf{K}(\mathbf{X}^o - \mathbf{H}\mathbf{X}^b) \quad (1)$$

where

$$\mathbf{K} = \mathbf{P}^b \mathbf{H}^T (\mathbf{H} \mathbf{P}^b \mathbf{H}^T + \mathbf{R})^{-1} \quad (2)$$

and where \mathbf{K} is the gain matrix, \mathbf{H} is the linear observation operator which maps the background state into the observational space, \mathbf{P}^b is the background error covariance. The analysis state vector \mathbf{X}^a is the new estimate of the state vector, which has the same dimension as the background field (\mathbf{X}^b), i.e. the current size of the AIRS vector. The size of the observation vector \mathbf{X}^o is determined by the size of assimilated observations (TES or MLS). The matrix \mathbf{R} is the observational error covariance. To prescribe \mathbf{R} , we assumed that there is no global bias in TES CO, nor global bias between AIRS and

Title Page

Abstract

Introduction

Conclusions

References

Tables

Figures

◀

▶

◀

▶

Back

Close

Full Screen / Esc

Printer-friendly Version

Interactive Discussion



TES CO. Since the variable amount is manageable and \mathbf{R} is assumed diagonal, we compute the inverse matrix in the gain matrix (i.e., \mathbf{K}) directly.

When we apply this data fusion algorithm, \mathbf{P}^b is the error covariance for the AIRS satellite retrievals. Satellite observations are often treated as spatially uncorrelated in data assimilation systems, but this is not strictly accurate (Talagrand, 1997). In the application of the data fusion technique, we assume a simple spatially decaying correlation that can be easily tuned by changing the correlation length scale, and comparing the results with in-situ data.

The background error covariance \mathbf{P}^b , consists of not only the correlation information between any two variables (at different locations) in the background state vector, but also the covariance matrices of the AIRS retrievals. It is defined as:

$$\mathbf{P}^b = \mathbf{D}^{1/2} \mathbf{C} \mathbf{D}^{1/2} \quad (3)$$

where \mathbf{C} is the matrix containing the correlations and \mathbf{D} is the matrix containing the variances of the analyzed species (El Amraoui et al., 2004). Here \mathbf{C} stands for the covariance between two grid points. We model the terms of \mathbf{C} with the quantity $C_{i,j} = \sigma_i \sigma_j \rho_h \rho_v$, where σ_i and σ_j are the standard deviations of background error at location i and j respectively, ρ_h is the horizontal correlation model, and ρ_v is the vertical correlation model. We use the power law for the ρ_h model as shown in Fig. 2 (left panel) (Dee and da Silva, 1999),

$$\rho_h = \left(1 + \frac{1}{2} \left(\frac{r}{L_0} \right) \right) \quad (4)$$

where r is the horizontal distance between two locations (i, j) , and L_0 is the prescribed horizontal error correlation length.

The vertical resolution of the analysis for the combined AIRS and TES CO is based on the AIRS pressure grid in the troposphere; whereas the vertical resolution of the analysis for AIRS and MLS CO is based on the AIRS pressure grid in the stratosphere and the UTLS regions. Table 1 lists all the pressure levels used in the AIRS and TES

Global carbon monoxide products

J. X. Warner et al.

Title Page	
Abstract	Introduction
Conclusions	References
Tables	Figures
◀	▶
◀	▶
Back	Close
Full Screen / Esc	
Printer-friendly Version	
Interactive Discussion	



combined CO (left columns) and the AIRS and MLS combined CO (right columns). These pressure levels are fixed except for near the surface. The vertical correlation model for AIRS and TES is shown in Fig. 2 (right panel) in the form

$$\rho_v = \exp(-\Delta y^2), \quad (5)$$

5 where

$$\Delta y = \frac{\ln P_n - \ln P_l}{L_z}. \quad (6)$$

P_n and P_l are the pressure values at level n and l ; and L_z is the prescribed vertical error correlation length (Daley and Barker, 2000).

10 In the examples given in Fig. 2, the horizontal correlation length $L_0 = 750$ km and the vertical correlation length $L_z = 0.17$ were chosen to match the measurement characteristics and sensitivities of AIRS and TES. Figure 3 shows the prescribed error standard deviations (SDVs) for AIRS (solid blue line), as the background error, and for TES (dashed red line), as the observational error. These errors originated from the retrieval error covariance matrices from the perspective teams and were averaged/smoothed
15 to form one global set of error profiles. We then adjusted these profiles to reduce prescribed errors for AIRS in the mid troposphere and for TES in the lower troposphere. This is based on previous knowledge and validation experience, which shows it is reasonable to place more emphasis on TES data in the lower troposphere and AIRS data in the mid-troposphere. Although we used 1-D background error SDVs as an approx-
20 imation for this study, the extension to 2-D error fields and the inclusion of seasonal variations is possible although not trivial.

4 Results

4.1 Combined AIRS and TES CO

We show in this section results from applying the data fusion methodology to AIRS and TES CO data. AIRS V5 L2 and TES V3 CO Volume Mixing Ratios (VMRs) at 500 hPa for 4 March 2006 are shown in Fig. 4 to demonstrate the data coverage pattern, where the squares represent AIRS footprints and the filled circles represent TES pixels. TES Step and Stare (SS) special observations (SO) were taken to coincide with the INTEX-B experiment (Singh et al., 2008) (<http://www.espo.nasa.gov/intex-b>). The pixel sizes do not represent the correct proportions of the sizes for the AIRS Field Of Regards (FORs) at approximately $45 \times 45 \text{ km}^2$ and the TES Field Of Views (FOVs) at $5 \times 8 \text{ km}^2$.

The vast majority of the AIRS pixels are not at nadir nor collocated with TES due to the coverage differences between the two sensors, so the data fusion scheme described in Sect. 3 is needed to distribute TES narrow swaths onto the global coverage of AIRS to produce daily maps. Results show that in vertical regions where AIRS has lower measurement sensitivity, the retrievals can still provide sufficient spatial variability (or patterns), even though they may not be able to produce the correct magnitude (see Fig. 4). Consequently, the TES CO profiles are distributed based on the AIRS variance horizontally.

We first demonstrate the overall performance of data fusion applied to global AIRS and TES CO data using the methodology described in Sect. 3. The monthly grid-averaged zonal means for March 2006 are shown in Fig. 5 for AIRS CO (left top panel), analysis CO (left middle panel), analysis increment (left bottom panel), and AIRS CO interpolated to TES locations (right top panel), TES CO (right middle panel), and Observation Minus Forecast (OMF) indicating TES minus AIRS in this experiment (right bottom panel), respectively. CO data are averaged in $1^\circ \times 1^\circ$ latitude and longitude grid boxes. The CO data range of the zonal mean analysis has increased significantly, especially in the lower troposphere, compared with the background AIRS CO values shown by the left column top two panels, as mirrored by the differences between TES

Title Page

Abstract

Introduction

Conclusions

References

Tables

Figures

◀

▶

◀

▶

Back

Close

Full Screen / Esc

Printer-friendly Version

Interactive Discussion



Global carbon monoxide products

J. X. Warner et al.

Title Page

Abstract

Introduction

Conclusions

References

Tables

Figures

◀

▶

◀

▶

Back

Close

Full Screen / Esc

Printer-friendly Version

Interactive Discussion



and AIRS on the right. This is an improvement over AIRS V5 CO retrievals based on previous studies (Warner et al., 2010; Yurganov et al., 2008). Quantatively, the analysis increment shows a decrease in the Southern Hemisphere (SH) lower troposphere of more than 40 ppbv and an increase in the Northern Hemisphere (NH) lower troposphere of as much as 40 ppbv. The analysis increment is minimal in the mid troposphere between 400 and 600 hPa to within ± 10 ppbv. There are also highly increased values of analysis increment at the tropics and decreased values at mid and high latitudes above 250 hPa in the UTLS.

The horizontal CO distribution at approximately 944 hPa from a monthly mean grid-averaged dataset for March 2006 is shown in Fig. 6 with TES CO (top panel), AIRS CO (middle panel), and the analysis CO (bottom panel). The analysis from the data fusion scheme presents much more realistic CO values based on our previous knowledge and validation results compared with the background CO values from AIRS. In particular, the CO analyses show distinct plumes in the NH associated with emissions and the SH shows the expected relatively low CO. The analysis CO agrees better with TES values, with higher CO values in the NH and lower values in the SH compared to AIRS, and it provides much better continuity in data coverage compared with TES CO values. Similarly, Fig. 7 shows the monthly mean grid-averaged CO distribution at approximately 506 hPa. Unlike at 944 hPa, the CO analysis distribution is very similar to the AIRS background CO. Note that these examples use monthly mean results to demonstrate the stability over time, the true advantage of this technique is the availability of daily maps when there are only a few narrow tracks per day from TES routine survey products.

For validation purposes, we have collocated the TES and AIRS footprints with the independent INTEX-B in situ measurements by selecting the retrievals from the nearest pixels. Figure 8 shows the curtain plots for CO VMRs along TES footprints for the DACOM CO measurements (top panel), TES V3 CO retrievals (second panel), AIRS V5 L2 CO retrievals (third panel), and the combined CO VMRs produced by data fusion (bottom panel). The geographical region measured on the DC-8 plane on that particu-

Global carbon monoxide products

J. X. Warner et al.

Title Page

Abstract

Introduction

Conclusions

References

Tables

Figures

◀

▶

◀

▶

Back

Close

Full Screen / Esc

Printer-friendly Version

Interactive Discussion



lar day was affected by agricultural fires in the southeast US, which resulted in high CO in the lower troposphere as shown by DACOM CO. AIRS V5 retrievals, using a single profile as the first guess, show good sensitivity in the mid troposphere (300–600 hPa), but the magnitudes of the retrieved results are lower by as much as ~ 40 ppbv below 900 hPa vertical level, in what is typically the boundary layer, due to reduced measurement sensitivity. TES senses higher CO signals in the lower troposphere especially over land (north of 30° N); however, TES shows lower CO values between 200 and 500 hPa over parts of the ocean by ~ 10–30 ppbv. Large portions of TES measurements show similar features as observed by DACOM in the lower troposphere where the AIRS observational signals are relatively weak. As shown on the bottom panel, the mid troposphere CO concentrations resemble AIRS retrievals in the mid troposphere while following the lower tropospheric CO values from TES. The combined products show higher CO VMRs in the lower troposphere, which improves the agreement with the in situ measurements to within 10–20 ppbv.

A profile validation against the DACOM in situ CO measurements is presented in Fig. 9. The DACOM in situ CO spiral profile used in this comparison was obtained during INTEX-B on 4 March 2006, near the center of the Gulf of Mexico, as denoted by a black square in Fig. 4 (Sachse et al., 1987). The CO VMR profiles are shown on the left panel in Fig. 9 as the in situ data (green), AIRS data (cyan), TES data (blue), and the combined AIRS and TES data (red). The combined profile agrees with the in situ profile much better than AIRS and TES profiles individually in the troposphere, especially over the vertical regions below 400 hPa. The combined profile is enhanced by AIRS in the mid troposphere by approximately 10–15 ppbv compared to TES and by TES below 75 hPa by nearly 20 ppbv. This shows the advantage of the data fusion method, in that it combines the best information characteristics from each sensor. The fact that the combined CO profile agrees with the in situ better than both AIRS and TES is largely due to the effect of the influence from neighboring pixels and from a different height region. The center panel shows AIRS AKs (averaging kernels), which indicate that the AIRS measurement information is primarily in the mid troposphere

peaking at approximately 500 hPa. The right panel shows TES AKs at three selected retrieval pressure levels (825, 510, and 215 hPa), indicating that, for this example, the maximum information responsible for the lower troposphere CO retrievals peak just above 900 hPa vertical level where the top of the boundary layer usually is (see blue line in right hand panel of Fig. 9). Although the final form of the AKs for the combined CO profiles, a nonlinear summation of the AKs from AIRS and TES, is not presented here, the combined information content should increase in the lower atmosphere based on the contribution from TES.

To extend our validation efforts, we compared the data fusion output with recently available in situ measurements from the HIAPER Pole-to-Pole Observations (HIPPO), which took place from January of 2009 to September 2011 (Wofsy et al., 2012). The CO merged 10-second best measurements are used (<http://hippo.ornl.gov/dataaccess>) (HIPPO_Merged_Data_Users_Guide_20121130). TES CO data is available for HIPPO-1 (8–30 January 2009) and HIPPO-2 (31 October–22 November 2009) flights, but not for HIPPO-3 (24 March–16 April 2010), HIPPO-4 (14 June–11 July 2011), and HIPPO-5 (9 August–9 September 2011) periods. We initially carried out this data fusion study when only TES V3 CO products were available, which apply to all results presented in earlier sections. Although newer TES CO products are available, the principle and advantages of the data fusion methodology still stands using TES V3 CO. We attempt, however, to demonstrate the full potential of the technique and use the latest TES V5 CO in the HIPPO validation.

Figure 10 shows a summary of the differences between the combined CO from AIRS and TES and CO from both HIPPO-1 and HIPPO-2 flights. The averaged differences (HIPPO – Retrievals) for all available cases are plotted at 41 vertical levels throughout the troposphere for AIRS (blue), TES (cyan), and for the combined product (red), respectively. Related error bars are computed from the 1-sigma standard deviations. The CO errors below 700 hPa are reduced by more than half, from 19.9 ppbv to 8.7 ppbv at 766 hPa and from 33.4 ppbv to 11.9 ppbv at 918 hPa. In the mid troposphere (350–600 hPa), TES average errors (10–14.3 ppbv) are twice as high as AIRS (–1.1––5.4 ppbv)

Global carbon monoxide products

J. X. Warner et al.

Title Page

Abstract

Introduction

Conclusions

References

Tables

Figures

◀

▶

◀

▶

Back

Close

Full Screen / Esc

Printer-friendly Version

Interactive Discussion



with similar SDVs. The errors for both AIRS and the combined AIRS and TES are below 5ppbv with AIRS retrieved CO lower than the HIPPO measurements and the combined CO slightly higher than HIPPO CO. The 1-sigma SDVs are approximately the same for AIRS CO and the combined AIRS and TES CO at $\sim 15\text{--}20$ ppbv in the mid troposphere; and reduced in the lower troposphere from $\sim 20\text{--}30$ ppbv to $\sim 10\text{--}20$ ppbv.

4.2 Combined AIRS and MLS CO retrievals

MLS CO retrievals are combined with AIRS CO using the same method as for AIRS and TES as described in Sect. 3. Livesey et al. (2007) describe the error characteristics of these retrievals, and recommend that data not be used below 215 hPa vertical level.

Although we are using a newer version (V3.3) of MLS data, based on the errors provided by MLS team (http://mls.jpl.nasa.gov/data/v3-3_data_quality_document.pdf), we choose to only use data above 215 hPa. We modified the data fusion methodology by using gridded data for AIRS and MLS as opposed to using L2 individual pixels in the case of AIRS and TES. AIRS CO retrievals are averaged into $3^\circ \times 3^\circ$ grids and MLS CO are averaged into $6^\circ \times 6^\circ$ grids, in both cases separated into daytime and nighttime measurements. This is done to reduce noise in the MLS CO data and to take into account that the MLS pixel represents a relatively long horizontal path due to limb viewing.

Figure 11 shows the global CO retrieval comparisons at 147 hPa for 4 March 2006 daytime only tracks, with AIRS V5 CO VMRs over-plotted by MLS in the upper panel and the combined AIRS and MLS CO VMRs in the lower panel. The combined AIRS and MLS CO fields show a large increase in their variability with higher CO at low latitudes by approximately 10 to 20ppbv or higher, and lower CO at mid and high latitudes (by ~ 10 ppbv) compared with the AIRS retrievals. Higher CO concentrations are identified as three large plumes over the tropics that cannot be measured by any nadir instrument; these features are expected due to the high tropopause and strong convection in the tropics. The decrease in CO values in the NH is also expected considering that the retrieved CO from a nadir-sensing instrument may be affected by the

Title Page

Abstract

Introduction

Conclusions

References

Tables

Figures

◀

▶

◀

▶

Back

Close

Full Screen / Esc

Printer-friendly Version

Interactive Discussion



higher tropospheric CO signals. It is difficult to resolve vertically the location of the high CO concentrations with thermal nadir viewing instruments, since the weighting functions for CO are generally broad and have very few (1–2) pieces of information in the troposphere.

Figure 12 shows the validation of the combined AIRS and MLS CO in the UTLS using in situ data from HIPPO flights. Measurements from all 5 HIPPO flights are summarized into the difference plot between HIPPO CO and the satellite products (HIPPO – Retrievals), shown as the blue curve for AIRS V5 CO, cyan curve for MLS CO, and the red curve for the combined AIRS and MLS CO in Fig. 12. The solid lines are the average errors showing 5 to 10 ppbv improvements for the height levels above 220 hPa over using AIRS data alone. The SDVs have been improved by approximately 5 ppbv, from 20–25 ppbv to 15–20 ppbv above 220 hPa. The MLS average error is very low (~ 2.1 ppbv) at 146.8 hPa, and it provides CO information to improve the combined products. In the same process, however, the SDVs are reduced from 18.9 ppbv to 16.7 ppbv compared to the MLS only CO. The MLS CO average error is relatively high (-17.8 ppbv) with SDVs at 36.0 ppbv at pressure level 215.4 hPa, which is given less weight in the data fusion of AIRS and MLS. The improvement of SDVs using the combined CO at 217.7 hPa over MLS CO is significant from 36.0 ppbv to 19.8 ppbv.

5 Summary

Multiple sensors (AIRS, TES, and MLS) on the A-train system make correlative CO measurements within a short time period (15–30 min). Based on differences between their measurement techniques, each sensor provides unique characteristics. This study seeks to combine these datasets without using a chemistry transport model, an approach that differs from traditional data assimilation. This approach, called data fusion, avoids uncertainties arising from model dynamics and transport issues, and provides a new set of measurements only from satellite sensors in that analysis is not dependent of model information. Results of this study have shown that the technique works well,

Global carbon monoxide products

J. X. Warner et al.

Title Page

Abstract

Introduction

Conclusions

References

Tables

Figures

◀

▶

◀

▶

Back

Close

Full Screen / Esc

Printer-friendly Version

Interactive Discussion



Global carbon monoxide products

J. X. Warner et al.

Title Page

Abstract

Introduction

Conclusions

References

Tables

Figures

◀

▶

◀

▶

Back

Close

Full Screen / Esc

Printer-friendly Version

Interactive Discussion



generally providing improved CO products compared with those from each individual sensor. The combined AIRS and TES CO products showed improvements of 10 to 40 ppbv and the combined AIRS and MLS CO products showed improvements of 10 to 20 ppbv above 175 hPa, based on validation using INTEX-B and HIPPO in situ measurements. The combined datasets retain the twice-daily nearly global coverage due to AIRS' wide swaths and the implementation of a cloud clearing algorithm that reconstructs cloudy pixels to recover more than 50 % of the daily measurements, compared to less than 10 % clear sky coverage.

This study provides a new framework to combine different measurements without the use of a model. We have demonstrated the feasibility of the data fusion technique using A-train measurements from AIRS, TES, and MLS. However, this technique can be easily adapted to include direct and in situ measurements and/or other satellite products, and take advantage of the mature approaches developed in the field of data assimilation. Further studies will examine in detail error estimation and the constraints provided by satellite products. Data fusion for other atmospheric species such as ozone and water vapor using this technique is also possible and should benefit chemical and dynamical studies of the UTLS.

Acknowledgements. This study was partially supported by the NASA Atmospheric Composition Program (NNX07AM45G), Climate Data Record Uncertainty Analysis (NNX11AL22A), and Modeling, Analysis and Prediction Program. We have also been partially supported by RTRA/STAE foundation from Toulouse, France. We acknowledge the AIRS, TES, and MLS Science Teams for the satellite products used in this study. We also thank the INTEX-B and HIPPO Science Teams for providing high quality in situ measurements.

References

Aumann, H. H., Chahine, M. T., Gautier, C., Goldberg, M., Kalnay, E., McMillin, L., Revercomb, H., Rosenkranz, P. W., Smith, W. L., Staelin, D., Strow, L., and Susskind, J.: AIRS/AMSU/HSB on the Aqua Mission: Design, Science Objectives, Data Products and Processing Systems, IEEE Trans. Geosci. Remote Sens., 41, 253–264, 2003.

Global carbon monoxide products

J. X. Warner et al.

Title Page

Abstract

Introduction

Conclusions

References

Tables

Figures

◀

▶

◀

▶

Back

Close

Full Screen / Esc

Printer-friendly Version

Interactive Discussion



- Beer, R.: TES on the Aura mission: scientific objectives, measurements, and analysis overview, *IEEE Trans. Geosci. Remote Sens.*, 44, 1102–1105, 2006.
- Crutzen, P. J. and Zimmermann, P. H.: The changing photochemistry of the troposphere, *Tellus*, 43AB, 136–151, 1991.
- 5 Dee, D. P. and da Silva, A. M.: Maximum-Likelihood estimation of forecast and observation error covariance parameters. Part I. Methodology, *Mon. Weather Rev.*, 127, 1822–1834, 1999.
- Hoor, P., Fischer, H., Lange, L., Lelieveld, J., and Brunner, D.: Seasonal variations of a mixing layer in the lowermost stratosphere as identified by the CO-O₃ correlation from in situ measurements, *J. Geophys. Res.*, 107, doi:10.1029/2000JD000289, 2002.
- 10 Hoor, P., Gurk, C., Brunner, D., Hegglin, M. I., Wernli, H., and Fischer, H.: Seasonality and extent of extratropical TST derived from in-situ CO measurements during SPURT, *Atmos. Chem. Phys.*, 4, 1427–1442, doi:10.5194/acp-4-1427-2004, 2004.
- Jiang, J. H., Livesey, N. J., Su, H., Neary, L., McConnell, J. C., and Richards, N. A.: Connecting surface emissions, convective uplifting, and long-range transport of carbon monoxide in the upper-troposphere: New observations from the Aura Microwave Limb Sounder, *Geophys. Res. Lett.*, 34, L18812, doi:10.1029/2007GL030638, 2007.
- 15 Kalnay, E.: *Atmospheric Modeling, Data Assimilation, and Predictability* (Cambridge University Press, Cambridge, 2002): pp. xxii + 341. ISBNs 0 521 79179 0, 0 521 79629 6., 2003.
- Lahoz, W. A., Khattatov, B., and Minar, R.: Data assimilation and information. *Data Assimilation: Making Sense of Observations*, edited by: Lahoz, W. A., Khattatov, B., and Minar, R., Springer, 3–12, 2010.
- 20 Lahoz, W. A., Orphal, J., Attié, J.-L., Chance, K., Liu, X., Edwards, D., Elbern, H., Flaud, J.-M., Claeys, M., and El Amraoui, L.: Monitoring air quality from space: The case for the geostationary platform, *B. Am. Meteorol. Soc.*, 93, 221–233, doi:10.1175/BAMS-D-11-00045.1, 2012.
- 25 Lin, M., Fiore, A., Horowitz, L. W., Cooper, O. R. R., Naik, V., Holloway, J. S., Johnson, B. J. J., Middlebrook, A. M., Oltmans, S. J. J., Pollack, I. B., Ryerson, T. B., Warner, J., Wiedinmyer, C., Wilson, J., and Wyman, B.: Transport of Asian ozone pollution into surface air over the western United States in spring, *J. Geophys. Res.*, 117, D00V07, doi:10.1029/2011JD016961, 2012.
- 30 Livesey, N. J., Filipiak, M. J., Froidevaux, L., Read, W. G., Lambert, A., Santee, M. L., Jiang, J. H., Pumphrey, H. C., Waters, J. W., Cofield, R. E., Cuddy, D. T., Daffer, W. H., Drouin, B. J., Fuller, R. A., Jarnot, R. F., Jiang, Y. B., Knosp, B. W., Li, Q. B., Perun, V. S., Schwartz,

Global carbon
monoxide products

J. X. Warner et al.

Title Page

Abstract

Introduction

Conclusions

References

Tables

Figures

◀

▶

◀

▶

Back

Close

Full Screen / Esc

Printer-friendly Version

Interactive Discussion



M. J., Snyder, W. V., Stek, P. C., Thurstans, R. P., Wagner, P. A., Avery, M., Browell, E. V., Cammas, J.-P., Christensen, L. E., Diskin, G. S., Gao, R.-S., Jost, H.-J., Loewenstein, M., Lopez, J. D., Nedelec, P., Osterman, G. B., Sachse, G. W., and Webster, C. R.: Validation of Aura Microwave Limb Sounder O₃ and CO observations in the upper troposphere and lower stratosphere, *J. Geophys. Res.-Atmos.*, 113, D15802, doi:10.1029/2007JD008805, 2007.

Luo, M., Beer, R., Jacob, D. J., Logan, J. A., and Rodgers, C. D.: Simulated observation of tropospheric ozone and CO with the Tropospheric Emission Spectrometer (TES) satellite instrument, *J. Geophys. Res.*, 107, doi:10.1029/2001JD000804, 2002.

Luo, M., Rinsland, C., Fisher, B., Sachse, G., Diskin, G., Logan, J., Worden, H., Kulawik, S., Osterman, G., Eldering, A., Herman, R., and Shephard, M.: TES carbon monoxide validation with DACOM aircraft measurements during INTEX-B 2006, *J. Geophys. Res.*, 112, D24S48, doi:10.1029/2007JD008803, 2007.

McMillan, W. W., Barnet, C., Strow, L., Chahine, M., Warner, J., McCourt, M., Novelli, P., Korontzi, S., Maddy, E., and Datta, S.: Daily Global Maps of Carbon Monoxide from NASA's Atmospheric InfraRed Sounder, *Geophys. Res. Lett.*, 32, L11801, doi:10.1029/2004GL021821, 2005.

McMillan, W. W., Evans, K. D., Barnet, C. D., Maddy, E. S., Sachse, G. W., and Diskin, G. S.: AIRS V5 CO Retrieval With DACOM In Situ Measurements, *IEEE Trans. Geosci. Remote Sens.*, 49, 1–12, ISSN: 0196-2892, doi:10.1109/TGRS.2011.2106505, 2011.

Pan, L. L., Randel, W. J., Gary, B. L., Mahoney, M. J., and Hints, E. J.: Definitions and sharpness of the extratropical tropopause: A trace gas perspective, *J. Geophys. Res.*, 109, D23103, doi:10.1029/2004JD004982, 2004.

Pan, L. L., Bowman, K. P., Shapiro, M., Randel, W. J., Gao, R.-S., Campos, T., Davis, C., Schauffler, S., Ridley, B. A., Wei, J. C., and Barnet, C.: Chemical behavior of the tropopause observed during the Stratosphere-Troposphere Analyses of Regional Transport (START) experiment, *J. Geophys. Res.*, 112, D18110, doi:10.1029/2007JD008645, 2007a.

Pan, L. L., Wei, J. C., Kinnison, D. E., Garcia, R. R., Wuebbles, D. J., and Brasseur, G. P.: A set of diagnostics for evaluating chemistry-climate models in the extratropical tropopause region, *J. Geophys. Res.*, 112, D09316, doi:10.1029/2006JD007792, 2007b.

Read, W. G., Lambert, A., Backmeister, J., Cofield, R. E., Christensen, L. E., Cuddy, D. T., Daffer, W. H., Drouin, B. J., Fetzer, E., Froidevaux, L., Fuller, R., Herman, R., Jarnot, R. F., Jiang, J. H., Jiang, Y. B., Kelly, K., Knosp, B. W., Pumphrey, H. C., Rosenlof, K. H., Sabouchi, X., Santee, M. L., Schwartz, M. J., Snyder, W. V., Stek, P. C., Su, H., Takacs, L. L., Thurstans,

Global carbon
monoxide products

J. X. Warner et al.

Title Page

Abstract

Introduction

Conclusions

References

Tables

Figures

◀

▶

◀

▶

Back

Close

Full Screen / Esc

Printer-friendly Version

Interactive Discussion



R. P., Vomel, H., Wagner, P. A., Waters, J. W., Webster, C. R., Weinstock, E. M., and Wu, D. L.: Aura Microwave Limb Sounder Upper Tropospheric and Lower Stratospheric H₂O and RHi Validation, *J. Geophys. Res.*, 112, doi:10.1029/2007JD008752, 2007.

Roger Daley and Edward Barker: NAVDAS Source Book 2000, NRL Atmospheric Variational Data Assimilation System, 2000.

Sachse, G. W., Hill, G. F., Wade, L. O., and Perry, M. G.: Fast-response, high-precision carbon monoxide sensor using a tunable diode laser absorption technique, *J. Geophys. Res.*, 92, 2071–2081, 1987.

Singh, H. B., Brune, W. H., Crawford, J. H., Jacob, D. J., and Russell, P. B.: Overview of the summer 2004 Intercontinental Chemical Transport Experiment-North, America (INTEX-A), *J. Geophys. Res.*, 111, D24S01, doi:10.1029/2006JD007905, 2006.

Susskind, J., Barnett, C. D., and Blaisdell, J. M.: Retrieval of atmospheric and surface parameters from AIRS/AMSU/HSB data in the presence of clouds, *IEEE Trans. Geosci. Remote Sens.*, 41, 390–409, 2003.

Sze, N. D.: Anthropogenic CO emissions: Implications for the atmospheric CO-OH-CH₄ cycle, *Science*, 195, 673–675, 1977.

Talagrand, O.: Assimilation of Observations, an Introduction. *J. Meteor. Soc. Japan*, 75, 191–209, 1997.

Warner, J. X., Wei, Z., Strow, L. L., Barnett, C. D., Sparling, L. C., Diskin, G., and Sachse, G.: Improved agreement of AIRS tropospheric carbon monoxide products with other EOS sensors using optimal estimation retrievals, *Atmos. Chem. Phys.*, 10, 9521–9533, doi:10.5194/acp-10-9521-2010, 2010.

Warner, J. X., Comer, M. M., Barnett, C. D., McMillan, W. W., Wolf, W., Maddy, E., and Sachse, G.: A Comparison of Satellite Tropospheric Carbon Monoxide Measurements from AIRS and MOPITT During INTEX-A, *J. Geophys. Res.*, 112, doi:10.1029/2006JD007925, 2007.

Waters, J. W., Froidevaux, L., Harwood, R. S., Jarnot, R. F., Pickett, H. M., Read, W. G., Siegel, P. H., Cofield, R. E., Filipiak, M. J., Flower, D. A., Holden, J. R., Lau, G. K., Livesey, N. J., Manney, G. L., Pumphrey, H. C., Santee, M. L., Wu, D. L., Cuddy, D. T., Lay, R. R., Loo, M. S., Perun, V. S., Schwartz, M. J., Stek, P. C., Thurstans, R. P., Boyles, M. A., Chandra, K. M., Chavez, M. C., Chen, G. S., Chudasama, B. V., Dodge, R., Fuller, R. A., Girard, M. A., Jiang, J. H., Jiang, Y., Knosp, B. W., LaBelle, R. C., Lam, J. C., Lee, K. A., Miller, D., Oswald, J. E., Patel, N. C., Pukala, Quintero, D. M. O., Scaff, D. M., Snyder, W. V., Tope, M. C., Wagner, P.

Global carbon monoxide products

J. X. Warner et al.

Title Page

Abstract

Introduction

Conclusions

References

Tables

Figures

◀

▶

◀

▶

Back

Close

Full Screen / Esc

Printer-friendly Version

Interactive Discussion



A., and Walch, M. J.: The Earth Observing System Microwave Limb Sounder (EOS MLS) on the Aura satellite, *IEEE Trans. Geosci. Remote Sens.*, 44, 1075–1092, 2006.

Wofsy, S. C., Daube, B. C., Jimenez, R., Kort, E., Pittman, J. V., Park, S., Commane, R., Xiang, B., Santoni, G., Jacob, D., Fisher, J., Pickett-Heaps, C., Wang, H., Wecht, K., Wang, Q.-Q., Stephens, B. B., Shertz, S., Watt, A. S., Romashkin, P., Campos, T., Haggerty, J., Cooper, W. A., Rogers, D., Beaton, S., Hendershot, R., Elkins, J. W., Fahey, D. W., Gao, R. S., Moore, F., Montzka, S. A., Schwarz, J. P., Perring, A. E., Hurst, D., Miller, B. R., Sweeney, C., Oltmans, S., Nance, D., Hints, E., Dutton, G., Watts, L. A., Spackman, J. R., Rosenlof, K. H., Ray, E. A., Hall, B., Zondlo, M. A., Diao, M., Keeling, R., Bent, J., Atlas, E. L., Lueb, R., and Mahoney, M. J.: HIPPO Merged 10-second Meteorology, Atmospheric Chemistry, Aerosol Data (R_20121129). Carbon Dioxide Information Analysis Center, Oak Ridge National Laboratory, Oak Ridge, Tennessee, USA, doi:10.3334/CDIAC/hippo_010, 2012.

Yurganov, L. N., McMillan, W. W., Dzhola, A. V., Grechko, E. I., Jones, N. B., and van der Werf, G. R.: Global AIRS and MOPITT CO measurements: Validation, comparison, and links to biomass burning variations and carbon cycle, *J. Geophys. Res.*, 113, doi:10.1029/2007JD009229, 2008.

Zahn, A., Brenninkmeijer, C. A. M., Maiss, M., Scharffe, D. H., Crutzen, P. J., Hermann, M., Heintzenberg, J., Wiedensohler, A., Gusten, H., Heinrich, G., Fischer, H., Cuijpers, J. W. M., and van Velthoven, P. F. J.: Identification of extratropical two-way troposphere-stratosphere mixing based on CARIBIC measurements of O₃, CO, and ultrafine particles, *J. Geophys. Res.*, 105, 1527–1535, 2000.

Global carbon monoxide products

J. X. Warner et al.

Title Page

Abstract

Introduction

Conclusions

References

Tables

Figures

◀

▶

◀

▶

Back

Close

Full Screen / Esc

Printer-friendly Version

Interactive Discussion



Table 1. The pressure levels used in AIRS (background and analysis) and TES (observations) combined CO (left columns), and AIRS and MLS combined CO (right columns).

Combined AIRS and TES CO		Combined AIRS and MLS CO	
Background	Observations	Background	Observations
1085.39343	1000.00	217.6866	215.4435
1056.51599	980.00	206.4598	146.7799
1028.04346	970.00	195.6079	100.0000
999.94598	941.20	185.1208	68.1292
972.26398	908.51	174.9984	46.4159
944.99750	825.40	165.2408	31.6228
918.12610	749.89	155.8378	21.5443
891.68030	681.29	146.7794	14.6790
865.63971	618.96	138.0756	10.0000
840.01459	562.34	129.7061	6.8129
814.80499	510.89	121.6711	4.6416
790.02087	464.16	113.9704	3.1623
765.64209	421.69	106.5838	2.1544
741.68878	383.11	99.5255	1.4678
718.16119	348.06	92.7782	1.0000
695.04901	316.22	86.3380	0.6813
672.36230	287.29	80.1977	0.4642
650.10120	261.01	74.3533	0.3162
628.26569	237.13	68.7966	0.2154
606.84552	215.44	63.5227	0.1468
585.85107	195.73	58.5243	0.1000
565.28198	177.82	53.7945	0.0464
545.13861	161.56	49.3260	0.0215
525.42078	146.77	45.1129	0.0100
506.11841	133.35	41.1481	0.0046
487.23141	121.15	37.4244	
468.78009	110.06	33.9348	
450.73410	100.00	30.5711	
433.11371		27.6263	
415.91891		24.7922	
399.12930		22.1638	
382.75519		19.7300	
366.78641		17.4867	
351.23300		15.4227	
336.09500		13.5320	
321.35220		11.8074	
307.01471		10.2399	
293.07239		8.8216	
279.53540		7.5450	
266.39359		6.4020	
253.63670		5.3848	
241.26500		4.4855	
229.28830		3.6961	
217.68660		3.0090	
206.45979		2.4164	
195.60789		1.9105	
185.12080		1.4837	
174.99840		1.1287	
165.24080		0.8379	
155.83780		0.6043	
146.77940		0.4208	
138.07561		0.2806	
129.70610		0.1771	
121.67110		0.1041	
113.97040		0.0554	
106.58380		0.0257	
99.52550		0.0095	
92.77820			
86.33800			
80.19770			

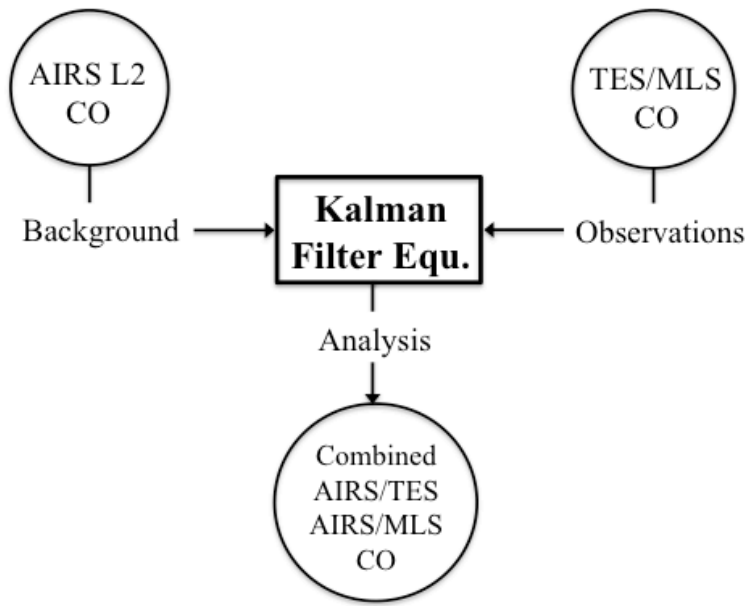


Fig. 1. Design of the satellite data fusion system, where AIRS operational V5 L2 retrievals are used as the background, and TES or MLS are added to the Kalman filter process as observations.

Global carbon monoxide products

J. X. Warner et al.

Title Page

Abstract Introduction

Conclusions References

Tables Figures

◀ ▶

◀ ▶

Back Close

Full Screen / Esc

Printer-friendly Version

Interactive Discussion



Global carbon monoxide products

J. X. Warner et al.

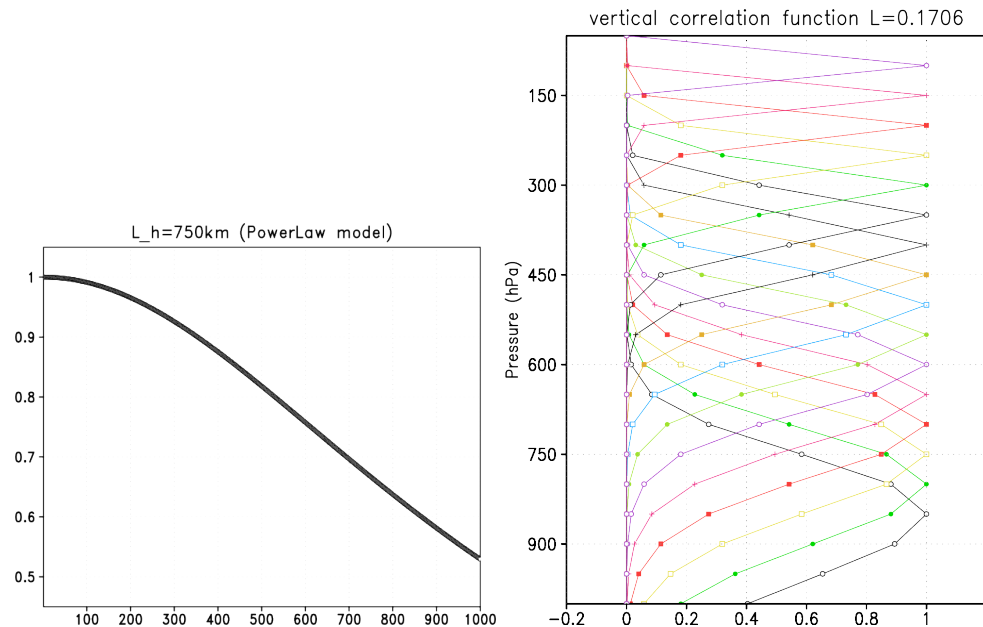


Fig. 2. (Right panel) Power law function with horizontal error correlation length of 750 km. (Left panel) Exponential function of the vertical error correlation with a length of 0.17.

[Title Page](#)[Abstract](#)[Introduction](#)[Conclusions](#)[References](#)[Tables](#)[Figures](#)[◀](#)[▶](#)[◀](#)[▶](#)[Back](#)[Close](#)[Full Screen / Esc](#)[Printer-friendly Version](#)[Interactive Discussion](#)

Global carbon monoxide products

J. X. Warner et al.

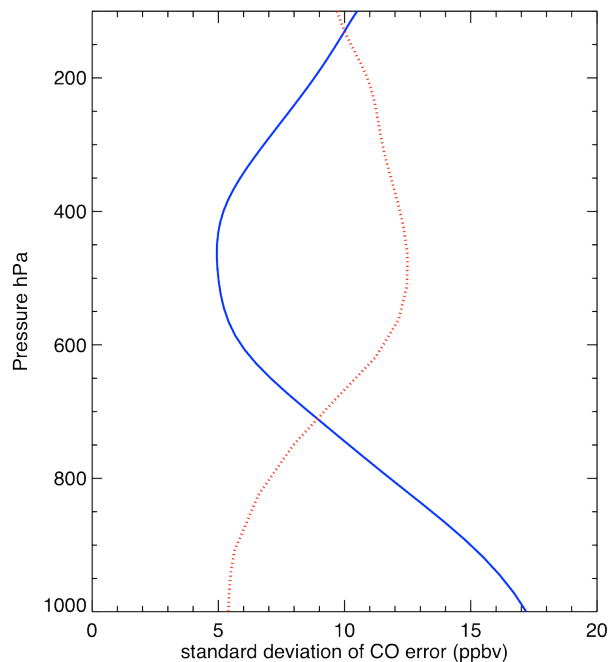


Fig. 3. Prescribed standard deviation of the CO error for AIRS (solid blue line) and TES (dashed red line).

[Title Page](#)[Abstract](#)[Introduction](#)[Conclusions](#)[References](#)[Tables](#)[Figures](#)[◀](#)[▶](#)[◀](#)[▶](#)[Back](#)[Close](#)[Full Screen / Esc](#)[Printer-friendly Version](#)[Interactive Discussion](#)

Global carbon monoxide products

J. X. Warner et al.

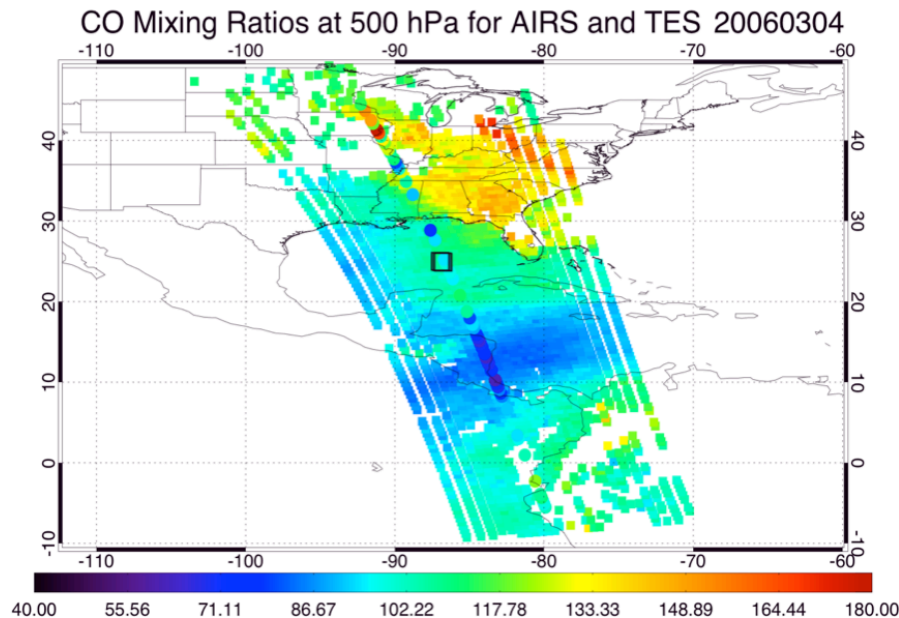


Fig. 4. The footprints of AIRS and TES special observations for 4 March 2006, where the squares represent AIRS CO mixing ratios at 500 hPa, the filled circles represent those for TES, and the black box outlines the location of the DC-8 in situ spiral profile.

[Title Page](#)[Abstract](#)[Introduction](#)[Conclusions](#)[References](#)[Tables](#)[Figures](#)[◀](#)[▶](#)[◀](#)[▶](#)[Back](#)[Close](#)[Full Screen / Esc](#)[Printer-friendly Version](#)[Interactive Discussion](#)

Global carbon monoxide products

J. X. Warner et al.

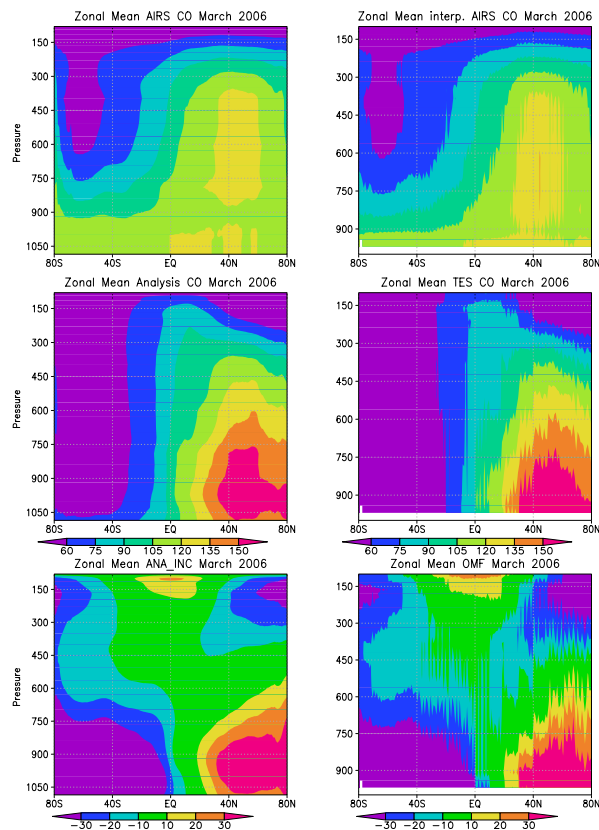


Fig. 5. Grid averaged monthly zonal means with AIRS CO (left top panel), analysis CO (left middle panel), analysis increment (left bottom panel), AIRS CO interpolated to TES location (right top panel); TES CO (right middle panel); and OMF showing TES minus AIRS CO (right bottom panel).

Global carbon monoxide products

J. X. Warner et al.

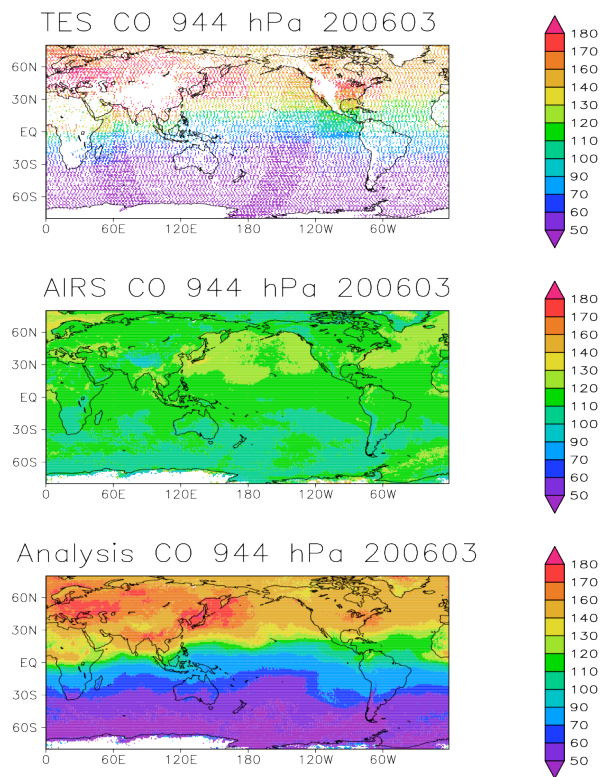


Fig. 6. Grid-averaged monthly mean CO distribution at approximately 944 hPa with TES CO (top panel), AIRS V5 CO (middle panel), and analyses CO (bottom panel).

Title Page

Abstract Introduction

Conclusions References

Tables Figures

◀ ▶

◀ ▶

Back Close

Full Screen / Esc

Printer-friendly Version

Interactive Discussion



Global carbon monoxide products

J. X. Warner et al.

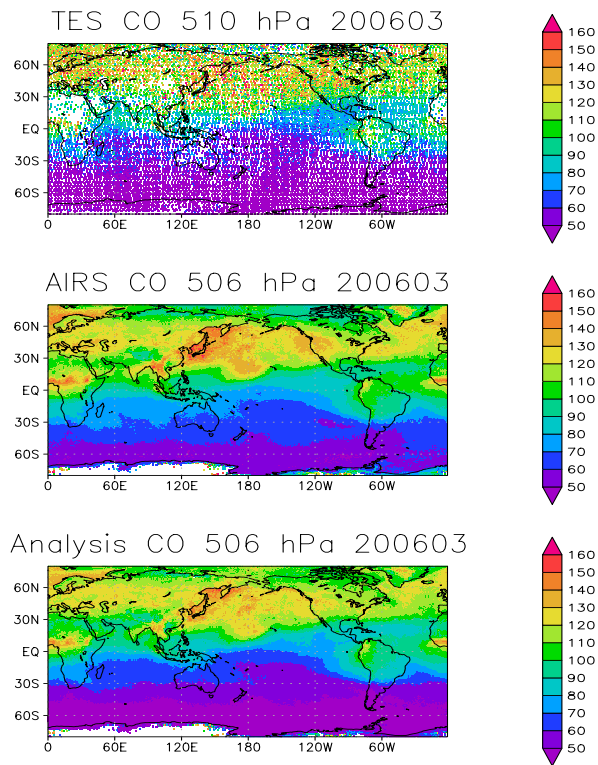


Fig. 7. Similar to Fig. 6 except at 506 hPa.

Title Page

Abstract Introduction

Conclusions References

Tables Figures

◀ ▶

◀ ▶

Back Close

Full Screen / Esc

Printer-friendly Version

Interactive Discussion



Global carbon monoxide products

J. X. Warner et al.

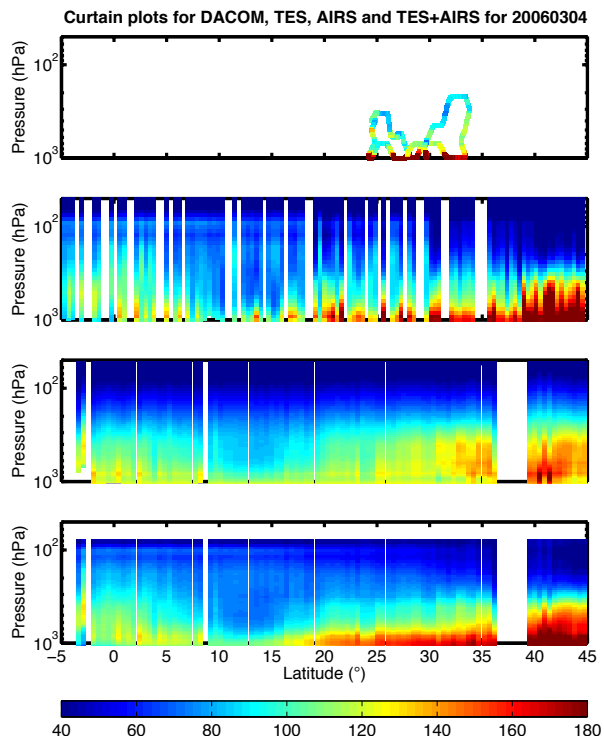


Fig. 8. Curtain plot validation against INTEX-B for AIRS and TES nadir pixels with DACOM CO (top panel), TES CO (2nd panel), AIRS CO (3rd panel), and analyses CO (bottom panel), respectively.

[Full Screen / Esc](#)[Printer-friendly Version](#)[Interactive Discussion](#)

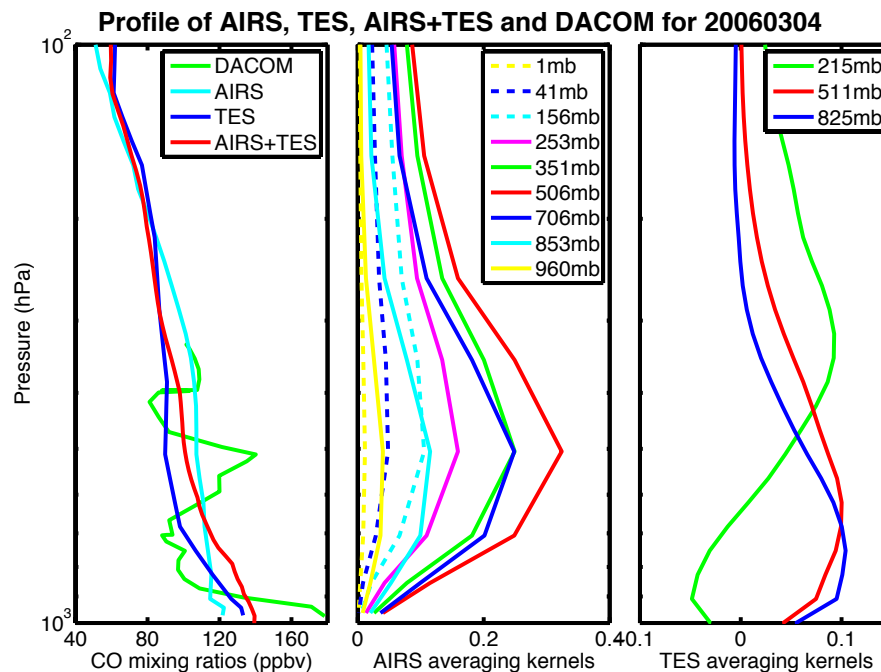


Fig. 9. A profile validation against the DACOM in situ CO measurements on 4 March 2006 (left hand panel) with DACOM CO (green curve), AIRS CO (cyan line), TES CO (blue line), and analyses CO (red line). Middle panel shows AIRS AKs and right hand panel shows TES AKs.

[Title Page](#)
[Abstract](#)
[Introduction](#)
[Conclusions](#)
[References](#)
[Tables](#)
[Figures](#)
[◀](#)
[▶](#)
[◀](#)
[▶](#)
[Back](#)
[Close](#)
[Full Screen / Esc](#)
[Printer-friendly Version](#)
[Interactive Discussion](#)


Global carbon monoxide products

J. X. Warner et al.

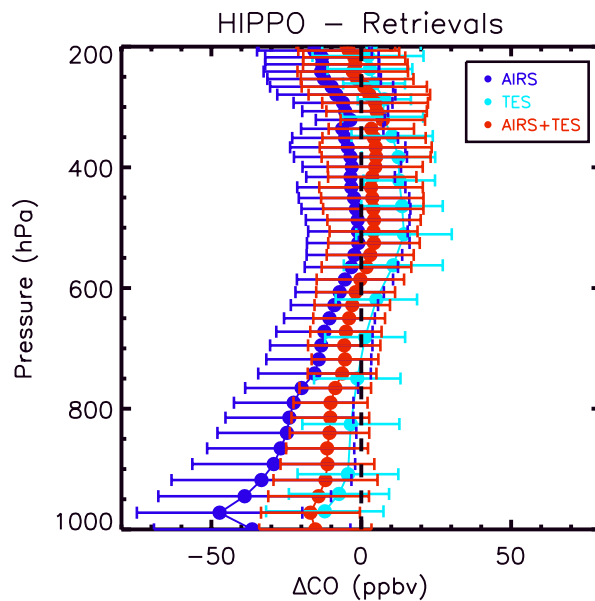


Fig. 10. CO from combined AIRS and TES validation against HIPPO showing (HIPPO-Retrievals) differences with 1-sigma SDVs.

[Title Page](#)[Abstract](#)[Introduction](#)[Conclusions](#)[References](#)[Tables](#)[Figures](#)[◀](#)[▶](#)[◀](#)[▶](#)[Back](#)[Close](#)[Full Screen / Esc](#)[Printer-friendly Version](#)[Interactive Discussion](#)

Global carbon monoxide products

J. X. Warner et al.

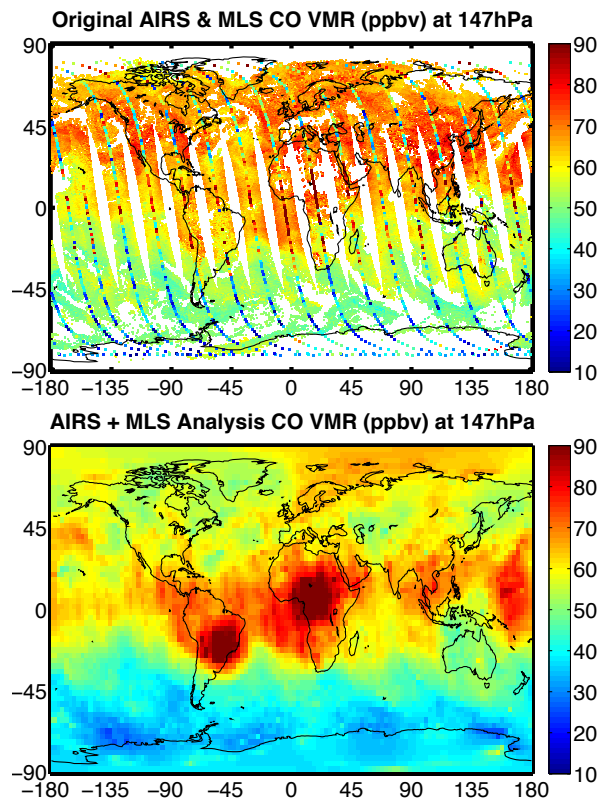


Fig. 11. Global CO retrieval comparisons at 147 hPa for 4 March 2006 daytime only tracks, with AIRS V5 CO VMRs over-plotted by MLS in the upper panel and the combined AIRS and MLS CO VMRs in the lower panel.

[Title Page](#)[Abstract](#)[Introduction](#)[Conclusions](#)[References](#)[Tables](#)[Figures](#)[◀](#)[▶](#)[◀](#)[▶](#)[Back](#)[Close](#)[Full Screen / Esc](#)[Printer-friendly Version](#)[Interactive Discussion](#)

Global carbon monoxide products

J. X. Warner et al.

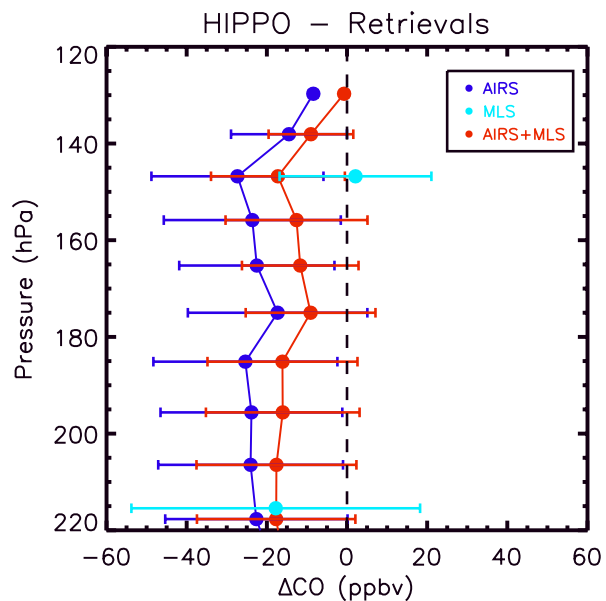


Fig. 12. Validation of the combined AIRS and MLS CO (red lines) in the UTLS regions using HIPPO (HIPPO – Retrievals) with 1-sigma SDVs, compared with AIRS CO (blue lines).

Title Page

Abstract

Introduction

Conclusions

References

Tables

Figures

◀

▶

◀

▶

Back

Close

Full Screen / Esc

Printer-friendly Version

Interactive Discussion

